




Hierarchical pomegranate-like MnO@N-doped carbon with enhanced conduction loss and interfacial polarization for tunable and broadband microwave absorption

Chenxu Wang¹, Jiawei Ding¹, Chuangchuang Gong¹, Tong Chen¹, Yijing Zhang¹, Kai Song¹, Chunsheng Shi^{1,2}, and Fang He^{1,2,*} 

¹School of Materials Science and Engineering and Tianjin Key Laboratory of Composites and Functional Materials, Tianjin University, Tianjin 300072, People's Republic of China

²Key Laboratory of Advanced Ceramics and Machining Technology of Ministry of Education, Tianjin University, Tianjin 300072, People's Republic of China

Received: 10 October 2022

Accepted: 21 November 2022

Published online:
14 December 2022

© The Author(s), under exclusive licence to Springer Science+Business Media, LLC, part of Springer Nature 2022

ABSTRACT

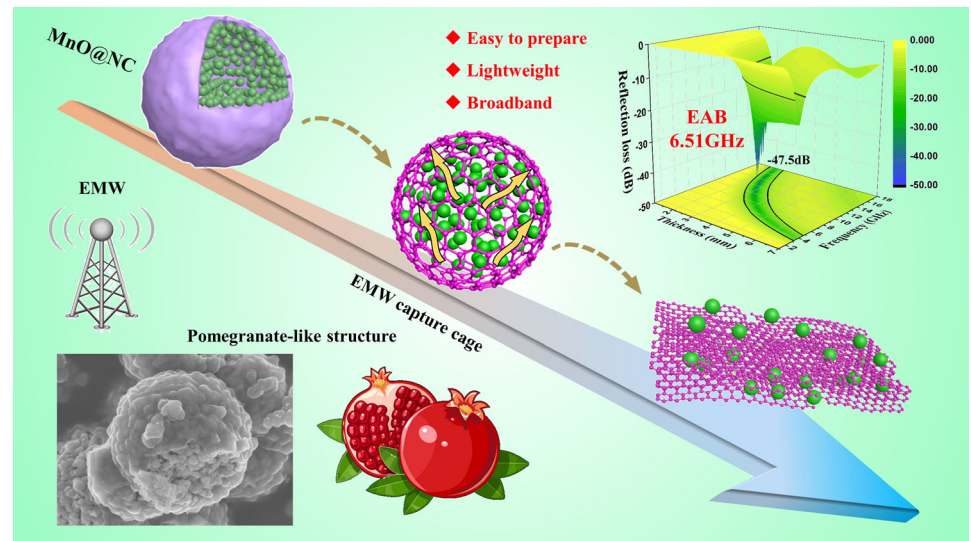
In order to tackle the electromagnetic pollution caused by the application of electromagnetic wave (EMW) in wireless communication, military industry, and other fields, broadband EMW absorption materials are urgently needed. To achieve this goal, emerging methods resort to constructing multivariate synergistic composites with unique morphology to enhance EMW absorption through diverse loss mechanisms and prominent structural advantage. Herein, a spatially tuned confinement pyrolysis strategy is proposed to design pomegranate-like MnO@NC absorption material. Unique hierarchical structure and more scattering sites are accessed via well-designed one-shell multiple cores nanostructure. N-doped carbon acts as an interwoven conductive network and restricts the movement of EMW in the shell, while nano-MnO acts as an impedance matching phase and interferes with the continuity of EMW. Moreover, the intercalation of dispersed MnO also amplifies the contribution of interfacial effect to EMW absorption, which can be verified by the calculation of the surface work function. The optimized composite possesses a maximum absorption bandwidth of 6.51 GHz at 2.4 mm and its maximum reflection loss reaches -58.4 dB ($d = 2.3$ mm). The synthesis of pomegranate-like composite provides a new direction for fabricating advanced carbonate-based EMW absorbers which are toward practical application.

Handling Editor: Naiqin Zhao.

Address correspondence to E-mail: fanghe@tju.edu.cn

<https://doi.org/10.1007/s10853-022-08008-8>

GRAPHICAL ABSTRACT



Introduction

The rapid development of aerospace equipment, wireless transmission, and high-frequency communication technology has made electronic equipment and component develop toward high integration and large power, which inevitably brings problems such as electromagnetic radiation and interference, seriously damaging the electromagnetic compatibility of equipment and the information security [1–3]. Lightweight and high-efficiency microwave absorbing material can effectively cut off the propagation path and reduce the secondary pollution of EMW, which has become a primary strategy to solve the problem of electromagnetic interference [4–8]. How to obtain stronger absorption and wider EMW response range under the premise of lightweight is an important issue that should be considered in the study of absorbing materials.

As one of conductive materials, carbon material with prominent conduction loss mechanism simultaneously exhibits low density, abundant morphology, and tunable character, so it has played a significant role in absorbing material [9–11]. Meanwhile, some polymer materials such as pyrrole, phenolic, and dopamine have adhesion and

uniformity when polymerizing, which have lower economic cost than carbon nanotube and graphene, and they have been used in the field of absorbing material [12–14]. However, excessive electrical conductivity of carbon will lead to total reflection of electric field wave. The current strategy is to construct multivariate carbon-based composite and use its synergistic effect to improve the incident behavior of EMW and enhancing its frequency applicability [15]. Excellent dielectric materials such as ZnO [16], TiO₂ [17], and CuS [18] have been used in composite engineering. Their compound not only improves the responsiveness to EMW, but also introduces heterogeneous interfaces. The greater the difference in electrical conductivity and dielectric property between the two phases forming the interface, the stronger the interface polarization effect [19]. MnO is a cost-effective dielectric material with the abundant resource. Its wide band gap (3.6 eV) leads to low conductivity [20]. These features make MnO an excellent substrate material for carbon material to suppress high EMW surface reflection behavior [21].

Taking into account the positional and structural relationship of the different components in the composite, structural engineering has significance in building advanced absorbers: (1) unique structures provide abundant heterointerfaces, which can

enhance the interface polarization; (2) the voids can adjust the impedance matching of the absorber; (3) enhanced EMW loss mechanism can also be obtained by structural engineering [22]. For example, meta-material-like property of cone-shaped hollow nanoarray structure can enhance reflection loss [23]. Different air layer thicknesses of yolk-shell would resonate with different frequencies for absorption [24]. Apart from this, flower-like Co/MnO@C [25], yolk-shell Ni@void@SnO₂(Ni₃Sn₂) [26], and hollow carbon microsphere [27] exhibited the property of structure-enhancing EMW attenuation ability. However, the construction of specific structures of the existing research usually requires complex processes such as sacrificial template method. Therefore, it is urgently needed to explore a simple process to fabricate complex structural material that is conducive to EMW absorption.

Herein, a “confined pyrolysis” method without sacrificing template was innovatively proposed. Pomegranate-like MnO@NC with micro–nano, core–shell, and porous structures was prepared by polymerization of dopamine and pyrolysis of MnCO₃. The uniformly dispersed MnO in the shell can form a dense EMW absorption network. Excellent conduction loss ability, strong interface polarization, and special EMW multiple absorption mechanism can be achieved by tuning the dielectric loss capability of MnO@NC and special design on the structure. Surprisingly, pomegranate-like MnO@NC has tunable and excellent EMW absorption properties. MnO@NC-650 possesses dual-band absorption property (C-band and Ku-band). Through enhanced conduction loss and interface polarization, the composite reaches the effective absorption bandwidth of 6.51 GHz, covering the Ku-band and part of the X-band. And it has an optimal reflection loss of –58.4 dB at 13.26 GHz and the thickness is only 2.3 mm. There is no doubt that the composite has the characteristics of excellent absorbing material with lightweight, strong absorption, and broadband. This work provides a research idea and basis for designing special structure absorbing materials based on carbonate to enhance EMW absorption.

Experiment section

Materials

The sodium bicarbonate (NaHCO₃) and manganese sulfate (MnSO₄) were purchased from Aladdin Shanghai Biological Technology Co., LTD., China. The dopamine hydrochloride (DA) was purchased from Shanghai Myrell Chemical Technology Co., LTD. The trimethylol aminomethane (Tris) was purchased from Tianjin Heowns Technology Co., LTD. The hydrochloric acid (HCl) was purchased from Tianjin Jiangtian Chemical Technology Co., LTD. All reagents used were analytical grade without further purification.

Synthesis of MnCO₃ spheres

The MnCO₃ spheres were prepared by a modified coprecipitation method [28]. One hundred and seventy-six mL of 12 mmol MnSO₄ and 35.2 mL of 12 mmol NaHCO₃ were dissolved separately in the mixed solution of deionized water and ethanol with a volume ratio of 10:1. Then, added the NaHCO₃ solution to the MnSO₄ solution and stirred for 3 h. The precipitate is separated and dried.

Synthesis of MnCO₃@PDA

0.6057 g of Tris was dissolved in 50 mL deionized water, adjust pH to 8.5 with 0.1 mol/L hydrochloric acid, and then add deionized water to 100 ml. The as-prepared MnCO₃ (160 mg) powders and dopamine hydrochloride (160 mg) were added to the Tris solution. After continuous stirring at room temperature for 24 h, the core–shell MnCO₃@PDA composite was collected after centrifugation. The final powders were washed with deionized water and dried under vacuum at 60 °C overnight.

Synthesis of MnO@NC

Pomegranate-like MnO@NC: Undergoing an annealing process in the Ar atmosphere for 100 min with heating temperature X °C (X = 650, 700, 750, 800), the as-prepared MnCO₃@PDA composites were transformed into the pomegranate-like MnO@NC. The heating rate is 7 °C min⁻¹. These samples are named as MnO@NC-X.

Hollow MnO@NC: The conditions are consistent with pomegranate-like MnO@NC-700 except that the holding time is 200 min. The hollow MnO@NC is named as MnO@NC-700H.

Characterization

X-ray diffraction was recorded by D8 Advance (Bruker) for determining the crystalline phase. The micromorphology, structure, and element distribution of the samples were characterized by field-emission scanning electron microscopy (SEM, HITACHI S-4800) and field-emission transmission electron microscopy (TEM, JEOLJEM-2010, 200 kV). The carbon atom bonding state of the samples was recorded using a LabRAM HR Raman spectrometer. The elemental composition and surface electronic states of samples were recorded by X-ray electron spectroscopy (XPS, Thermo ESCALAB 250XI). Specific surface area and pore size distribution were collected on a BET analyzer (QuantaGrome US). The

work function of different planes for N-doped carbon and MnO was calculated by the Material studio software based on the density function theory (DFT).

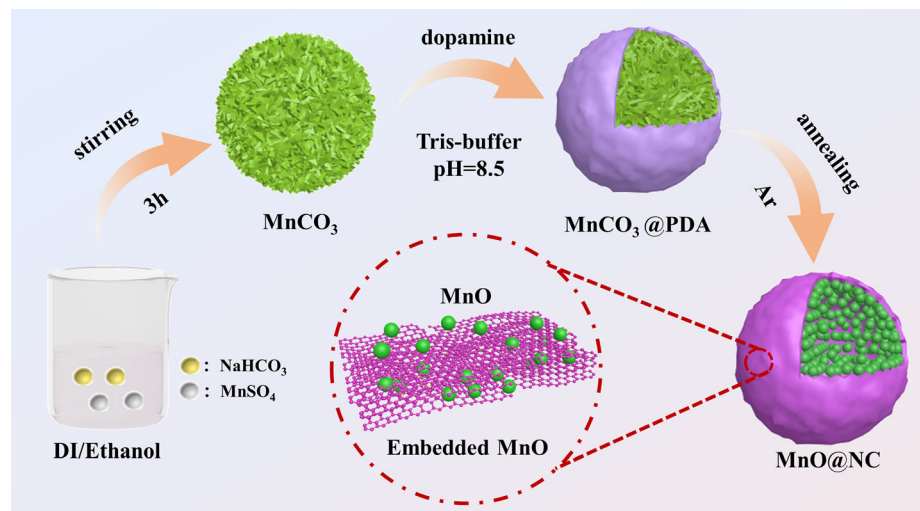
For the measurement of electromagnetic parameters, the samples were mixed with paraffin wax in a certain proportion (45 wt%) to form a ring with an outer diameter of 7.00 mm and an inner diameter of 3.04 mm. The electromagnetic parameters were measured through the Agilent PNA-5244 Avector network analyzer within frequency of 1–18 GHz.

Results and discussion

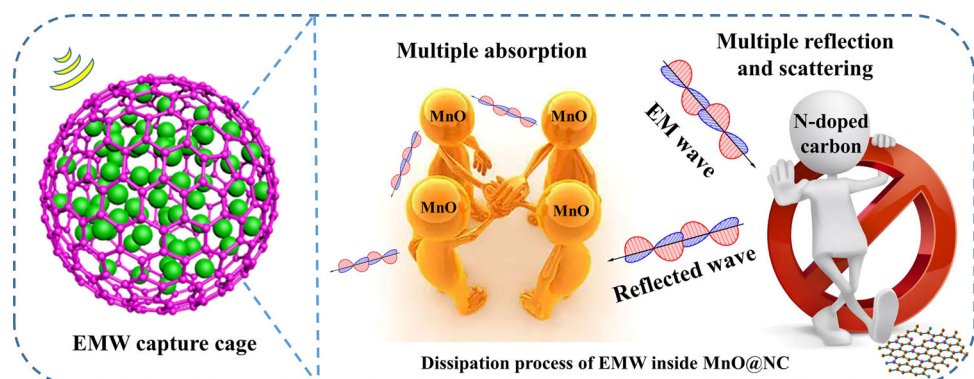
Preparation and characterization of MnO@NC

The preparation process of MnO@NC is shown in Scheme 1. Firstly, NaHCO_3 and MnSO_4 were dissolved in a mixture of deionized water and ethanol, and then stir to obtain MnCO_3 microsphere. Next,

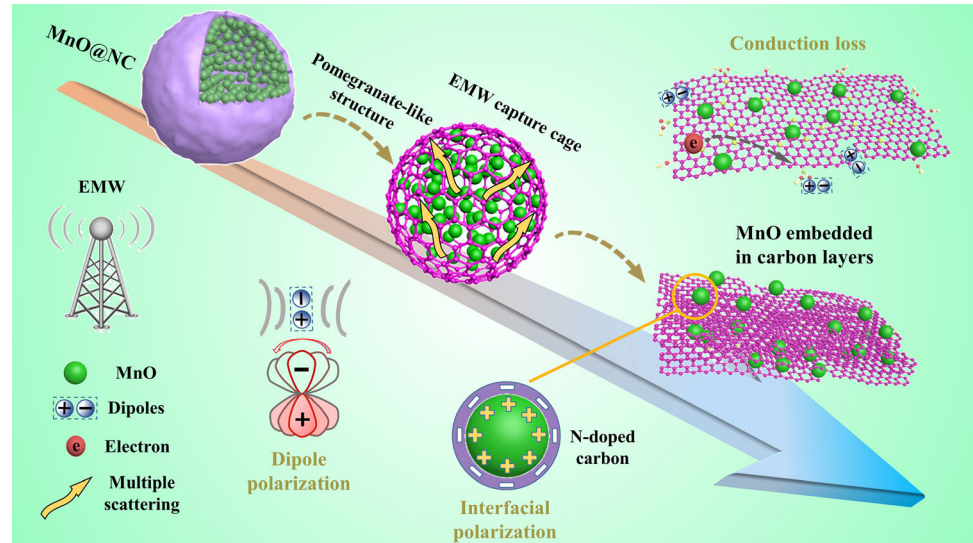
Scheme 1. Schematic diagram for the synthesis process of pomegranate-like MnO@NC composites.



Scheme 2 Schematic illustration of the electromagnetic trapping cage mechanism of pomegranate-like MnO@NC.



Scheme 3 Schematic of the EMW absorption mechanisms for pomegranate-like MnO@NC composite.



MnCO₃ was coated by dopamine self-polymerizing in Tris solution (pH = 8.5) to fabricate core-shell MnCO₃@PDA. Finally, the prepared MnCO₃@PDA composite was further annealed in the Ar atmosphere.

The microstructure of the samples was characterized by SEM and TEM. As shown in Fig. 1, the MnO@NC samples show typical pomegranate-like morphology. Most of the MnO particles are separated from each other and uniformly coated by carbonized dopamine (Fig. 1c). It should be pointed out that MnCO₃ (Fig. S1) shows microsphere structure with sharp corner which possesses a uniform size of 1.35 μm. Interestingly, the sharp corners become rounded after being wrapped by layer of PDA (Fig. S2).

The specific formation process is depicted as follows: The observed MnCO₃ microspheres are formed by the nucleation, growth, and assembly of many grains [28]. After annealing process, MnCO₃ microspheres were decomposed into MnO and CO₂. Due to the weak binding force at the grain boundary, the decomposition reaction will take place first from the relatively weak grain boundaries. At the same time, the decomposition reaction causes volume shrinkage resulting in the separate particles. But the dense carbon shell derived from carbonization of dopamine will limit the release of CO₂ [29], resulting in hierarchical microstructure that MnO particles in the outer layer are in contact with the carbon shell while exhibiting an individual structure internally (Fig. S3). Figure S5a shows the MnO particles formed after the

pyrolysis of MnCO₃, without the confinement of the carbon shell, the MnO particles grow to several microns and are randomly distributed, which proves the feasibility of the confinement pyrolysis strategy in the preparation of special morphology [30].

From Fig. 1b–d and Fig. 1e–g, the external morphology of MnO@NC does not obviously change with temperature, but the voids between the pomegranate seeds-like MnO particles increase. At the same time, the MnO particles diameter became significantly larger, and some MnO particles gradually were embedded in the carbon shell, and then MnO@NC presents a hollow structure, such as MnO@NC-800 (Fig. 1d and g). The reason is that with the increase in temperature, the driving force of diffusion increases. The MnO particles aggregate and grow up in order to reduce the surface energy, finally diffuse outward [31]. However, due to the confinement of the carbon shell, the MnO particles can only embed in carbon shell, resulting in enlarged voids (Fig. 1a). Multiple particles are intercalated into amorphous carbon to create the heterogeneous interface. Its HRTEM image (Fig. 1h) displays that the lattice spacing is 0.256 nm, which exactly matches the (111) crystal plane of MnO (JCPDS No.77-2363). The EDS elemental mapping of MnO@NC-700 in Fig. 1i shows the uniform coating of carbon around MnO. The N element contained in dopamine is doped into the carbon shell after annealing process, which can significantly enhance the dipole polarization and carrier mobility, then improve the EMW absorption.

As shown in Fig. 2a, the phase characterization of the samples at each preparation stage was obtained by XRD. The three main peaks are located at $2\theta = 24.25^\circ$, 31.36° , and 51.48° corresponding to the (012), (104), and (018) crystal planes of MnCO_3 (JCPDS No.44-1472), respectively, indicating the successful synthesis of MnCO_3 . Coated dopamine did

Figure 2 a XRD patterns of as-prepared samples; b Raman spectra of MnO@NC (650, 700, 800); XPS spectra: c C 1s, d N 1s, e Mn 2p, and f O 1s of the MnO@NC-700 ; g N_2 adsorption–desorption isotherm of MnO@NC (650, 700, 800); h pore size distribution of MnO@NC (650, 700, 800).

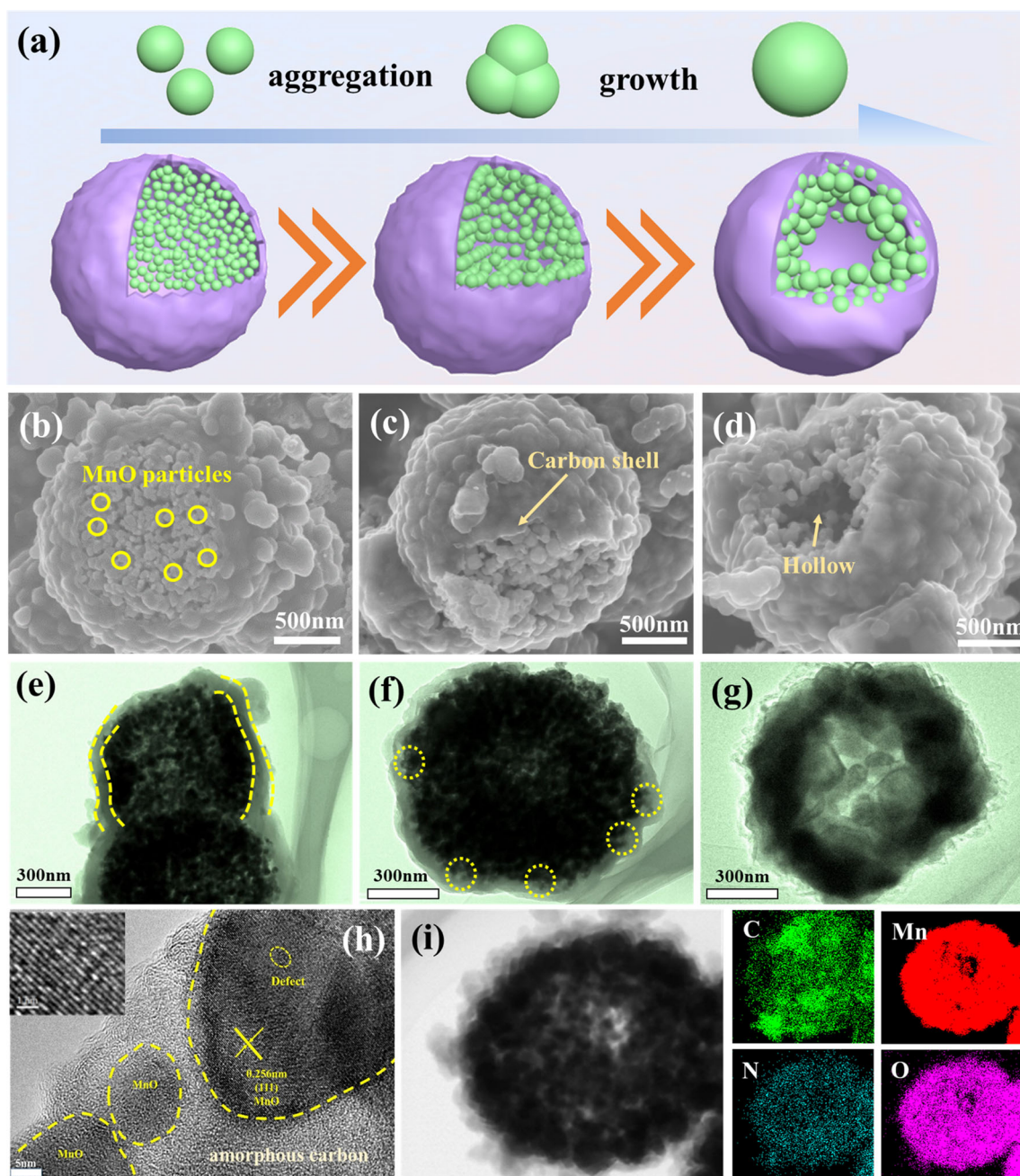
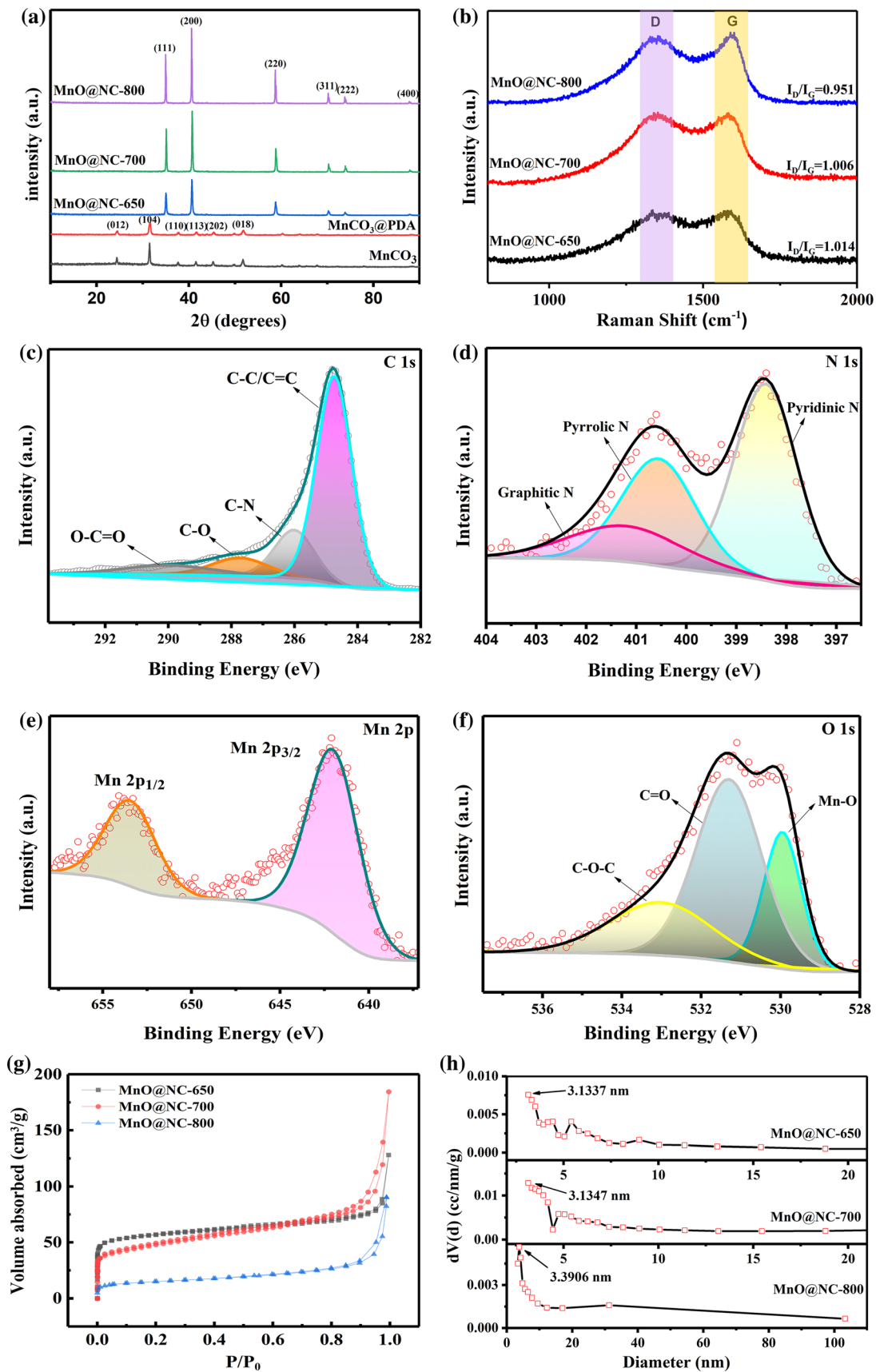


Figure 1 a Schematic diagram of structural change of MnO@NC , SEM and TEM images of (b, e) MnO@NC-650 , (c, f) MnO@NC-700 , (d, g) MnO@NC-800 ; h HRTEM image of MnO@NC-700 ; i elements mapping images of MnO@NC-700 .



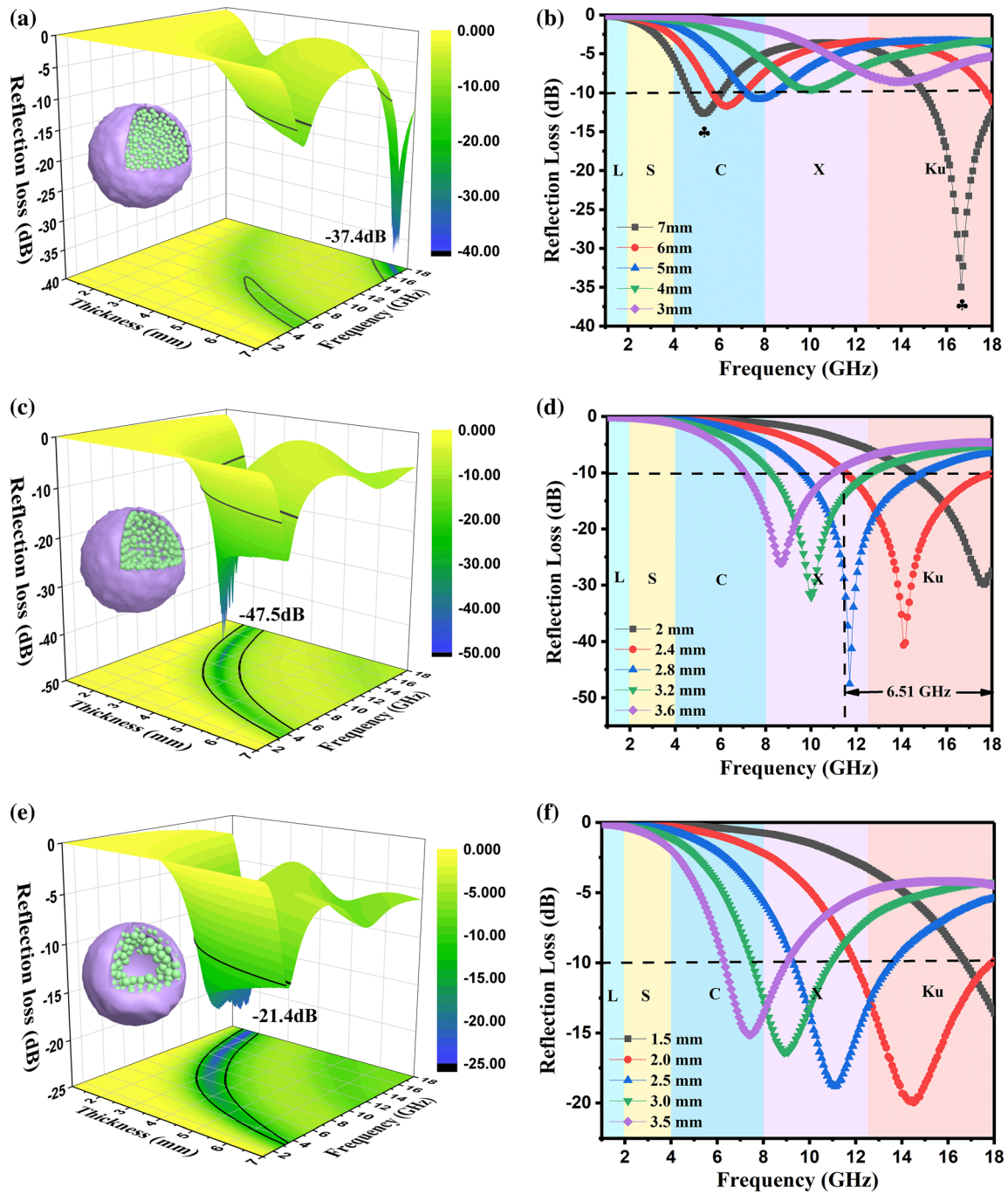


Figure 3 Three-dimensional plots of the frequency dependence of MnO@NC: **a** 650, **c** 700, and **e** 800; RL curves of MnO@NC: **b** 650, **d** 700, and **f** 800.

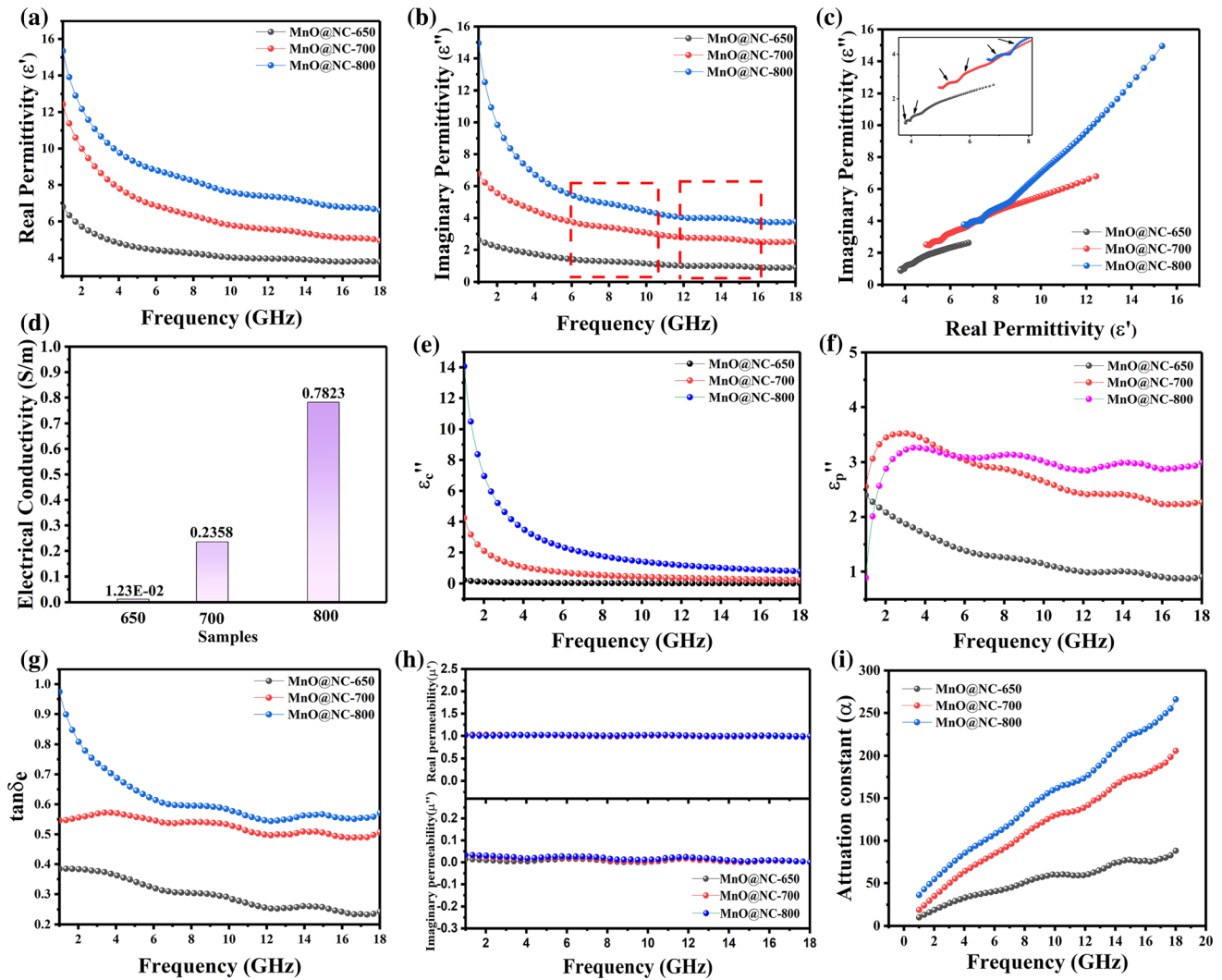


Figure 4 a Real part and b imaginary part of the relative complex permittivity; c typical Cole–Cole plot; d electrical conductivity (45%); e ϵ_c'' and f ϵ_p'' g $\tan \delta_e$, h permeability, and i the attenuation constant (α) of MnO@NC (650, 700, 800).

not cause changes in the crystalline phase. The existing form of carbon will be further characterized by Raman and XPS. After annealing process, it was found that all the MnO@NC samples have the same diffraction peaks at $2\theta = 34.94^\circ, 40.56^\circ, 58.71^\circ, 70.18^\circ, 73.80^\circ,$ and 87.78° which match to the (111), (200), (220), (311), (222), and (400) planes of the MnO (JCPDS No.77-2363), respectively. The better crystallinity of the MnO nanoparticles was illustrated by the sharper diffraction peak with the increase in the calcination temperature. The grain diameters with different temperature (650, 700, 800), which can be obtained by the Debye–Scherrer formula, are

20.8 nm, 23.1 nm, and 39.2 nm, respectively. It confirms the growth behavior of MnO, that is the primary fine MnO particles generated by the pyrolysis of MnCO_3 will aggregate and grow in the subsequent high-temperature environment, resulting in the change of the pomegranate voids.

Raman spectroscopy can accurately characterize the bonding state and defect of carbon. The state of carbon atom is very critical to the EMW absorption performance because it affects the electromagnetic parameters of the composite. As shown in Fig. 2b, two distinct peaks near 1340 cm^{-1} and 1580 cm^{-1} correspond to D-band and G-band of carbon,

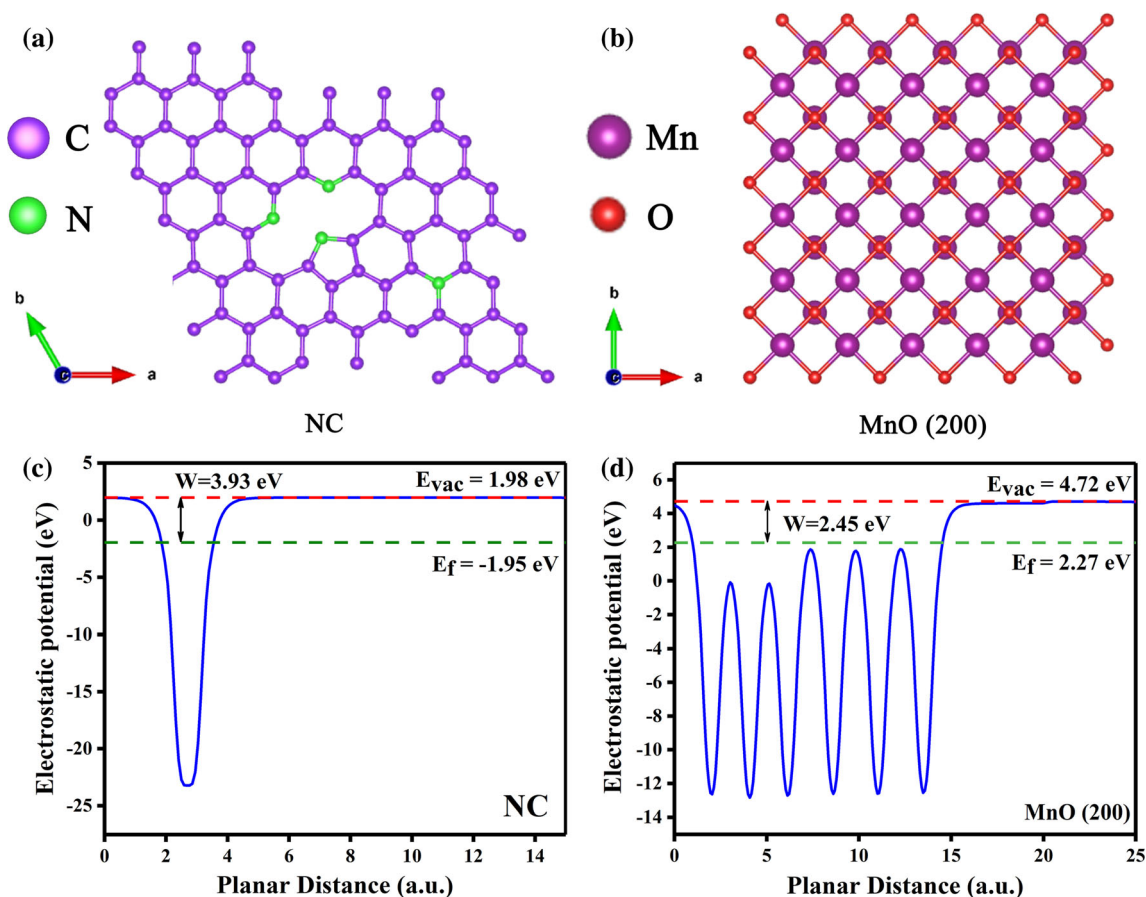


Figure 5 First-principles calculations of the work functions. **a** Model of N-doped carbon and **b** MnO crystal plane used in the calculation for the work function; **b**, **c** the work function obtained by calculating the typical crystal planes between the sample interface.

respectively [32, 33]. The ratio of I_D/I_G is closely related to the disorder degree of carbon material. It can be seen that the I_D/I_G value of MnO@NC composites shows a trend of decreasing, indicating an increase in the degree of graphitization. But the higher I_D/I_G value indicates that there are still a lot of defects in the carbon, benefit for dipole polarization loss. The elemental electronic state and composition of the sample surface were further analyzed by XPS. As shown in Fig. 2c–f, the peak of C, N, O, and Mn is shown clearly, respectively. The high-resolution XPS spectrum of C is deconvoluted into the C–C/C=C (284.7 eV), C–N (285.7 eV), C–O (287.6 eV), and O–C=O (289.4 eV) species, respectively [34, 35]. The high-resolution XPS spectrum of N 1s shows three peaks at 398.1 eV, 400.2 eV, and 401.2 eV, which correspond to the pyridinic N, pyrrolic N, and graphitic N [36]. Pyrrolic N and pyridine N contribute to

enhanced polarization and graphitic N contributes to conduction loss [37]. The $Mn2p_{3/2}$ and $Mn2p_{1/2}$ peaks of Mn^{2+} at 641.2 eV and 653 eV are clearly distinguished, indicating the successful synthesis of MnO [38, 39]. For O 1s spectrum displays peaks at 531.5 eV and 533.0 eV, matched to C=O and C–O–C groups [40]. Further, another peak at 529.8 eV is accepted as Mn–O [41].

To further probing the effect of MnO growth behavior on structure, the pore size and specific surface area of these samples were characterized by N_2 adsorption and desorption isotherm. As shown in Fig. 2g, h, all isotherms possess a distinct combination of type-I and type-IV curves and display a sharp increase at low relative pressure, indicating the presence of diverse pore structure [15, 42]. According to the BJH model, the main pore size of these samples is about 3–4 nm. The macro-porous appear as the

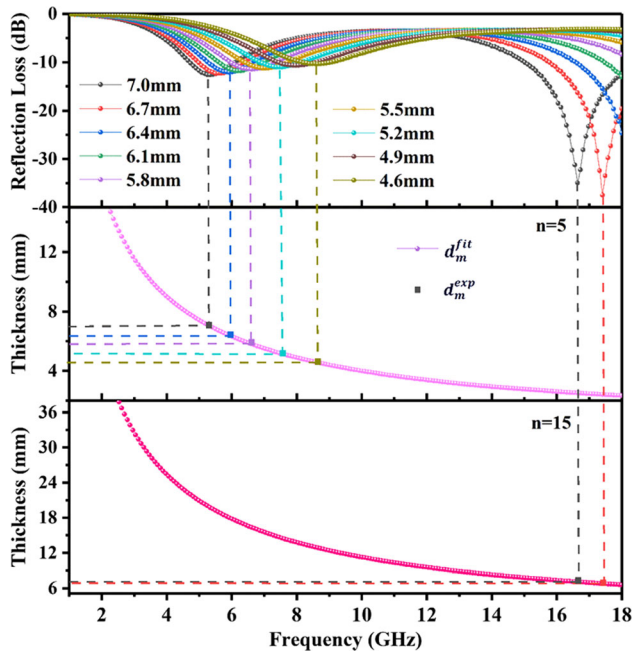


Figure 6 Dependence of $\lambda/4$ matching thickness versus RL peak plots of MnO@NC-650.

MnO grow (Fig. 2h, MnO@NC-800), similar to the result obtained by SEM and TEM. As calculated by the BET method, the specific surface areas of these MnO@NC samples are $216.4 \text{ m}^2 \text{ g}^{-1}$, $169.3 \text{ m}^2 \text{ g}^{-1}$, and $52.8 \text{ m}^2 \text{ g}^{-1}$, respectively. This further confirms that the temperature affects the pore size and specific surface area of samples as affecting the growth behavior of MnO.

EMW absorbing properties of MnO@NC

To assess the EMW absorption capability of the MnO@NC, the reflection loss (RL) value was calculated by transmission line theory:

$$Z_{in} = Z_0 \sqrt{\frac{\mu_r}{\epsilon_r}} \tanh\left(j \frac{2\pi f d}{c} \sqrt{\mu_r \epsilon_r}\right) \quad (1)$$

$$RL(\text{dB}) = 20 \log \left| \frac{Z_{in} - Z_0}{Z_{in} + Z_0} \right| \quad (2)$$

where Z_{in} is the normalized input impedance of the absorber. Z_0 is the free space impedance. ϵ_r ($\epsilon_r = \epsilon' - j\epsilon''$) and μ_r ($\mu_r = \mu' - j\mu''$) represent the complex permittivity and complex permeability, respectively. f is the test frequency of the EMW. c is the speed of light. d is the thickness of the absorber. Generally, the standard for effective absorption is $RL < -10 \text{ dB}$. As shown in Fig. S6, pure MnO shows the RL value of no more than -8 dB , which is due to its poor attenuation ability. Although the EMW can fully enter into the MnO particles, the inability to attenuate the EMW completely transmits it out. However, after composited with carbon, a noticeable improvement in the EMW absorption capability was observed. Figure 3 shows 3D RL images and 2D RL curves from 1 to 18 GHz for MnO@NC at different thicknesses. Among them, MnO@NC-700 exhibits the best absorbing performance. The RL_{\min} of MnO@NC-700 is -47.5 dB at 11.65 GHz with a thickness of 2.8 mm and the effective absorption bandwidth is 6.51 GHz (11.49–18 GHz) at 2.4 mm. By adjusting the thickness, full-band absorption of 2.2–18 GHz is achieved. In other samples, surprisingly, MnO@NC-650 has a rare dual-band absorption performance, which can

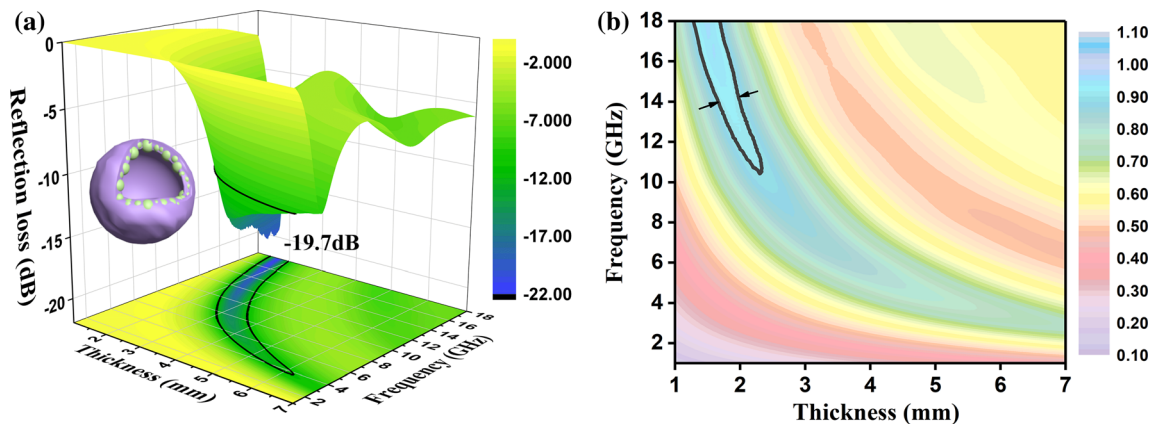


Figure 7 Three-dimensional RL of **a** MnO@NC-700H, two-dimensional impedance matching (Z) of **b** MnO@NC-700H.

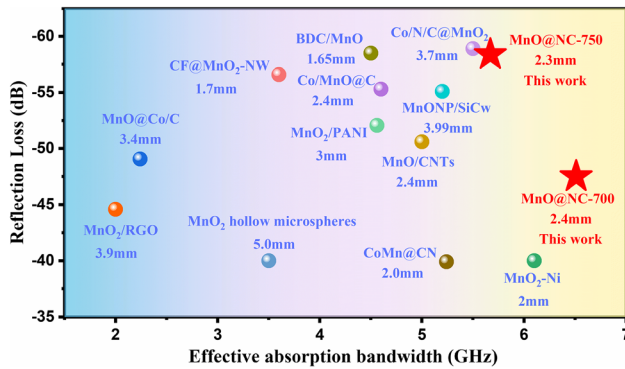


Figure 8 EMW absorption of the composites containing manganese oxide in recent literature.

simultaneously absorb C-band and Ku-band EMW under the same thickness. However, its thickness cannot meet the need for application. Compared with MnO@NC-700, MnO@NC-800 exhibited a decreased RL_{\min} of -21.4 dB due to excessive skin effect, but its optimum reflection loss occurs at a thinner thickness (1.5 mm). Therefore, by adjusting structure and inherent property, this composite can achieve tunable absorption performance, which can be a competitive candidate for efficient absorbers.

The electromagnetic parameters were measured to analyze the EMW absorption property of different MnO@NC samples. Figure 4a and b shows the real (ϵ') and imaginary (ϵ'') parts of the complex permittivity (ϵ_r) at 1–18 GHz. The ϵ' component of ϵ_r represents the energy storage capacity of the EMW, while the ϵ'' represents the EMW dissipation capacity of the absorber. The average value of ϵ' increases from 4.35 to 6.55 and finally to 8.43, and the average ϵ'' value increases from 1.33 to 3.49 and then to 5.39. The ϵ'' values of these samples varied in the range of 2.62–0.92, 6.79–2.50, and 14.96–3.78, respectively. The changing trend of the ϵ'' curve is very obvious. This phenomenon is called frequency dispersion which is characteristic of conduction loss. The reason is that with the frequency of EMW increase, the cross-sectional area of induced current will decrease, the resistance increases, so the value of the conductive loss decreases [43]. Not only that, all samples exhibit two broad resonance peaks in the frequency range of 1–18 GHz, suggesting that different types of attenuation may exist. Different EMW loss mechanisms can be further confirmed by the Cole–Cole plots, which are based on Debye theory:

$$\left(\epsilon' - \frac{\epsilon_s + \epsilon_\infty}{2}\right)^2 + (\epsilon'')^2 = \left(\frac{\epsilon_s - \epsilon_\infty}{2}\right)^2 \quad (3)$$

wherein ϵ_s and ϵ_∞ represent the static and relative dielectric permittivity at infinite frequencies respectively. Each semicircle corresponds to one Debye relaxation process [44]. As shown in Fig. 4c, all samples show two obvious semicircles, consistent with the resonance peaks in the ϵ'' curves, which are derived from interface polarization and dipole polarization. The special pomegranate-like steric configuration will generate a large number of heterogeneous interfaces in the contact between the seed and the shell. The difference in dielectric property between MnO (Fig. S5) and the carbon shell is very significant which creates a strong twisting electric field, causing strong polarization to dissipate EMW. From Fig. 2b and Fig. 2d, electronegativity due to N doping and defects in carbon leads to dipole relaxation behavior. The alternating electric field in EMW is periodically acted on the dipole (defect and doped N) in turn, causing them to move with the properties of the electric field. As the frequency of the electric field increases, their changes gradually fail to keep up with the change in frequency, thus acting as a “drag” to the electric field, dissipating the energy of the EMW. Apart from the two semicircles, the Cole–Cole plots also present an obvious straight line in the tail, indicating that conductive loss originating from the conductive carbon network in the MnO@NC absorber should not be neglected [45]. The higher slope and the longer tail of the line indicate that conduction loss increases [46].

In order to further explore the intrinsic EMW absorption capability of MnO@NC composite, the direct contribution of polarization (ϵ''_p) and conductivity (ϵ''_c) to the ϵ'' were calculated, the formula follows as [47]:

$$\epsilon'' = \epsilon''_p + \epsilon''_c = (\epsilon_s - \epsilon_\infty) \frac{2\pi f \tau}{1 + (2\pi f)^2} + \frac{\sigma}{2\pi f \epsilon_0} \quad (4)$$

σ is the conductivity of the absorber. ϵ_0 is the vacuum permittivity. τ is the relaxation time. As shown in Fig. 4e, in the process of structural tuning, the change of temperature leads to the improvement of conduction loss ability. The ϵ''_c of MnO@NC-650 hardly contributes to the EMW attenuation, indicating that polarization is the main source of its

absorption performance. But it still has a smaller ϵ_p'' value. Considering the structure, defects, and N doping of MnO@NC, it believes that the heterointerface behavior caused by the structural change is the main contribution to its polarization effect [48]. Compared with MnO@NC-650, increased temperature can provide a stronger driving force for the diffusion of MnO. More MnO particles will be embedded in the carbon shell, resulting in more heterointerfaces, so the remaining samples have stronger interface polarization effect (Fig. 4f). In the 1–18 GHz frequency range, ϵ_c'' has a large contribution to the dielectric loss in the low-frequency band, while in the middle- and high-frequency bands, the ϵ_p'' have a larger magnitude of the contribution to the dielectric loss. The reason for this phenomenon is that, on the one hand, the pomegranate structure has a larger heterojunction area than the traditional face to face contact, which can have a stronger electromagnetic response at the interface; on the other hand, the uniform coating of dopamine establishes efficient electrical conductivity network, which facilitates the transport of charge carriers. But in the high-frequency alternating electric field, there will be higher inductive reactance and more serious skin effect, which leads to the decline of the ability of conduction [49]. The combination of polarization and conduction loss results in high dielectric loss capability, which can be confirmed in $\tan\delta_e$. Considering that the composite has no magnetic contribution (Fig. 4h), it can be considered that the attenuation capability is all derived from the dielectric loss.

$$\tan \delta_e = \frac{\epsilon''}{\epsilon'} \tag{5}$$

$$\alpha = \frac{2\pi f}{c} \sqrt{(\mu''\epsilon'' - \mu'\epsilon') + \sqrt{(\mu''\epsilon'' - \mu'\epsilon')^2 + (\mu''\epsilon' + \mu'\epsilon'')^2}} \tag{6}$$

$\tan\delta_e$ represents the dielectric loss capability, and α is the attenuation coefficient representing the attenuation capability of the absorber to EMW. It can be seen that they are gradually increasing, indicating why the composite tends to be thinner. It is worth noting, as mentioned above: Firstly, only the degree of graphitization reaches a certain value, the composite material can have a considerable conduction loss capacity, this is why only increase 50 °C can make MnO@NC-700 have a higher loss capacity. Secondly, because pore storage of air reduces the

effective dielectric constant (ϵ_{eff}), properly counteracts the effect of ϵ_c'' increase on EMW attenuation ability [50].

To further illustrate the structural relationship between MnO and carbon shell, the microscopic topography of MnO@NC-700 etched by HCl is shown in Fig. S8. Without the support of MnO particles, the carbon shell will be broken, which shows that there is not only a surface-to-surface contact, but an embedded relationship between MnO and N-doped carbon. In order to qualitatively illustrate the contribution of the interfacial polarization induced by the heterointerface to the EMW absorption performance, the surface work functions of N-doped carbon and MnO (200) crystal planes were calculated by DFT. Figure 5a and b presents the models of crystal plane of N-doped carbon and MnO which are used in the calculation for the work function. The work function of N-doped carbon surface is 3.93 eV (Fig. 5c), and for MnO (Fig. 5d), the work function of MnO-(200) plane is only 2.45 eV. The huge difference of the work function (1.48 eV) between the N-doped carbon/MnO-(200) interface will lead to a large accumulation of charges on the interface (tend to N-doped carbon which has larger work function). Under the alternating electric field of EMW, the carriers collide continuously, during which EMW energy is dissipated [51, 52].

But only high attenuation capacity does not mean good EMW absorption performance. It is well known that the impedance matching determines whether the EMW can be incident in the absorber. The formula is as follows [53]:

$$Z = \left| \frac{Z_{in}}{Z_0} \right| \tag{7}$$

When Z is equal to 1, all microwave can be incident without reflection, while impedance mismatch causes the EMW to be totally reflected at the absorber/air interface [54]. The range highlighted by the black line in Fig. S9 is the region with good impedance matching (0.9–1.1), indicating that EMW can be effectively incident inside the material. It is obvious that the area with good impedance matching shows a trend of first increasing and then decreasing. Compared with other samples, MnO@NC-700 has the best impedance matching, which is the direct reason for its wide bandwidth. Not only due to suitable electrical conductivity, but also the internal homogeneous

structure has an improved effect on the incident behavior of EMW. Compared with the agglomerated and segregated MnO particles, the uniformly dispersed MnO particles play a tuning dispersion function on the EMW in the entire range of microsphere, so that the impedance is closer to the free space. Apparently, MnO@NC-700 exhibits better EMW absorption performance due to the strong dielectric loss capability brought about by more uniform heterojunction and proper conduction loss capability, as well as the improved impedance matching from the uniformly graded garnet-like structure.

Different from the previous, the as-prepared MnO@NC-650 can effectively absorb both C-band and Ku-band EMW at the same thickness, which can be attributed to the interference loss. When the EMW reflected at the absorber/air interface and the absorber/backplane interface have a phase difference of $(2n + 1)\pi$, the EMW will be attenuated by interference. The corresponding formula is as follows:

$$d_m = \frac{2n + 1}{4} \frac{c}{f(|\mu_r||\epsilon_r|)^{1/2}} \quad (n = 0, 1, 2, \dots) \quad (8)$$

d_m is the matching thickness. That is when the thickness of the absorber is $(2n + 1)/4$ times of the wavelength of the EMW, the mutual cancellation of the reflected wave and the incident wave will occur. Generally speaking, better impedance matching characteristics will appear at odd multiples of a quarter wavelength [43]. As shown in Fig. 6, it is found that the value of n is different when the C-band ($n = 5$) and the Ku-band ($n = 15$) satisfy the quarter-wavelength model, while the matching thickness is same. This particular phenomenon is closely related to electromagnetic parameter. The dielectric constant of low-frequency EMW with the same matching thickness is greater than that of high-frequency EMW, and the relationship satisfies:

$\epsilon_{\text{low}} = \epsilon_{\text{high}} * \left(\frac{f_{\text{high}}}{f_{\text{low}}} * \frac{2n_{\text{low}} + 1}{2n_{\text{high}} + 1} \right)^2$, so that when designing an absorber that is known to meet dual-frequency absorption at specified thickness, the electromagnetic parameters of the material that meet dual-band absorption can be predicted in advance through the exhaustive substitution of n values [55].

Structure selection engineering of MnO@NC

It is found that the dispersion of MnO can be regulated by the growth behavior of MnO. To illustrate the advantages of the pomegranate-like structure engineering in EMW absorption, hollow MnO@NC was prepared under the same heat treatment condition but extended holding time as a comparison, as shown in Fig. S10a and Fig. S10b. Prolonging the holding time will give fine MnO sufficient energy to aggregate and grow to form a hollow structure. XRD image (Fig. S10d) and Raman spectrum (Fig. S10e) show the same phase composition and graphitization degree as MnO@NC-700. Compared with other samples, MnO has grown sufficiently, and the grain size calculated according to the Debye Scherrer formula is 42.1 nm. The N_2 adsorption and desorption isotherm and pore size distribution of the MnO@NC-700H are shown in Fig. S10f. The reduction in the amount of absorbed N_2 at low pressure and the appearance of the hierarchical pore structure further confirmed the successful construction of the hollow microporous structure, implying that most of MnO particles are completely embedded in the carbon shell. As a result, the MnO@NC composite under the sufficient growth of MnO was successfully obtained, thereby exploring the effect of the dispersion behavior of MnO on the absorption performance.

Figure 7a shows the RL of MnO@NC-700H, the composite has a maximum RL of -19.7 dB at 17.4 GHz and the optimal effective bandwidth reaches 6 GHz at 2.0 mm, which is much lower than the EMW absorption performance of pomegranate-like MnO@NC-700. Not only that, the impedance match of MnO@NC-700H is far inferior to that of pomegranate-like composite. On the one hand, it is found that MnO@NC-700H and MnO@NC-700 have almost identical electrical conductivity (Table. S1), suggesting that conduction loss is not a major factor responsible for the difference in their performance. On the other hand, for the pomegranate-like structure, the more uniform dispersion of MnO in the carbon shell provides stronger interfacial polarization, but is not much different from MnO@NC-700H. These further illustrate the dominant role of the structure in optimizing EMW absorption.

The pomegranate-like structure has uniform and dense MnO particles inside, the particles are separated to form complex and uniform pores benefit to

area contact with air. The outer layer has a larger heterojunction interface promote to outstanding interfacial polarization. When EMW is incident on the surface of the MnO@NC microspheres from the outside, the good impedance matching will allow more EMW to enter, thereby reducing the reflected wave. When the EMW is incident in, the effects of different components should be specifically considered. The N-doping carbon with high electrical conductivity will limit the propagation range of the EMW, making it multiple reflection and scattering inside the carbon shell, which plays a role in confinement. MnO is a material with low dielectric property. During the multiple reflection and scattering process, the EMW is repeatedly embedded and extracted from multiple MnO particles. Each heterogeneous transmission will cause a certain amount of EMW loss, thus playing a multiple absorption role. In addition, the MnO particles form a dense coupling network, which destroys the continuity of the EMW, changes the phase of the propagating EMW, and then makes the EMW more likely to interfere. Pomegranate-like MnO@NC acts as an electromagnetic trapping cage to “capture” and “consume” EMW, in which N-doping carbon plays a role in trapping and MnO particles play a role in absorption (Scheme 2). Compared with the traditional solid core-shell structure, the 3D porous pomegranate-like structure undoubtedly has a lower density, which provides a prerequisite for lightweight. The uniform pomegranate-like structure matched with the enhanced interfacial polarization and conduction loss contributes to the efficient broadband absorption performance.

EMW dissipation mechanism of MnO@NC

Figure 8 shows the EMW absorption property of composites containing manganese oxide in recent literature [13, 20, 25, 56–64]. Compared with the reported absorbents, pomegranate-like MnO@NC composite has a better reflection loss, a wider effective absorption bandwidth, and more lightweight characteristic, demonstrating that it can serve as a promising material in the field of EMW absorption. Scheme 3 displays the diverse EMW dissipation mechanisms of pomegranate-like MnO@NC. In conclusion, its excellent EMW absorption performance comes from three aspects: (i) Prominent structural endow MnO@NC with a special electromagnetic

response mechanism: The 3D porous pomegranate-like structure makes improvement to the incident behavior of the EMW and increases scattering sites. The outer highly conductive carbon shell limits the propagation range of the EMW, and the inner dense MnO coupling network breaks the EMW continuity and improves the electromagnetic energy absorption efficiency. (ii) Strong interfacial polarization effect: Multiple MnO particles are embedded in the carbon shell, resulting in a larger heterointerface area. The huge difference in the ability of the two to capture electrons makes the electrons accumulate at the heterointerface, which makes the electric field energy of the EMW convert into heat energy at the interface. (iii) Establishment of 3D conductive networks: The dense encapsulation of dopamine provides a channel for carrier migration, and the highly conductive dopamine after carbonization provides a high conduction loss capability, which directly leads to the lightweight property.

Conclusion

In conclusion, this work introduces a confinement pyrolysis strategy that cleverly exploits the inherent reactions of material to design a special structure. Pomegranate-like MnO@NC composite with unique hierarchical structure, large specific surface area, abundant heterointerfaces, and abundant N doping was synthesized via the pyrolysis of MnCO₃ and the polymerization of dopamine. The optimized EMW absorption performance can be accessed by tuning dielectric property and micromorphology. It was found that the MnO@NC-700 exhibits the maximum effective absorption bandwidth of 6.51 GHz and the MnO@NC-750 exhibits the best reflection loss of –58.4 dB. The response mechanisms to EMW come from the following points: The uniform deposition of dopamine promotes conduction loss. The fine MnO particles embedded in the carbon layer enhance the interface polarization, which is verified by calculating the surface work function difference of the heterointerface. Besides, special morphology endows it with “electromagnetic trapping cage” absorption mechanism and better impedance matching. The interface polarization and conduction loss can be matched through simple process adjustment, and at the same time, excellent tunable wave absorption performance can be achieved by taking advantage of the

outstanding structure. It is believed that this confinement pyrolysis strategy with structural advantages and diverse loss mechanisms opens the door for microstructure engineering to enhance absorption.

Acknowledgements

The authors acknowledge the financial support by the National Natural Science Foundation of China (Grant No. 51972226 and No. 52172222) and National Natural Science Foundation of Tianjin City (Grant No. 16JCZDJC36600).

Data availability

All data needed to evaluate the conclusions in the paper are present in the paper and/or Supplementary Materials. Data and materials may be requested from C.X.W. and F.H (corresponding authors).

Declarations

Conflict of interest The authors declare that they have no known competing financial interests or personal relationships that could have appeared to influence the work reported in this paper.

Ethical approval Our experiments do not involve human tissue.

Supplementary Information: The online version contains supplementary material available at <https://doi.org/10.1007/s10853-022-08008-8>.

References

- [1] Iqbal A, Shahzad F, Hantanasirisakul K, Kim M-K, Kwon J, Hong J, Kim H, Kim D, Gogotsi Y, Koo CM (2020) Anomalous absorption of electromagnetic waves by 2D transition metal carbonitride Ti_3CNT_x (MXene). *Science* 369:446–450
- [2] Shahzad F, Alhabeab M, Hatter CB, Anasori B, Man Hong S, Koo CM, Gogotsi Y (2016) Electromagnetic interference shielding with 2D transition metal carbides (MXenes). *Science* 353:1137–1140
- [3] Song Q, Ye F, Yin X, Li W, Li H, Liu Y, Li K, Xie K, Li X, Fu Q, Cheng L, Zhang L, Wei B (2017) Carbon nanotube-multilayered graphene edge plane core-shell hybrid foams for ultrahigh-performance electromagnetic-interference shielding. *Adv Mater* 29:1701583
- [4] Wen C, Li X, Zhang R, Xu C, You W, Liu Z, Zhao B, Che R (2022) High-density anisotropy magnetism enhanced microwave absorption performance in $Ti_3C_2T_x$ MXene@Ni microspheres. *ACS Nano* 16:1150–1159
- [5] Xu X, Shi S, Tang Y, Wang G, Zhou M, Zhao G, Zhou X, Lin S, Meng F (2021) Growth of NiAl-layered double hydroxide on graphene toward excellent anticorrosive microwave absorption application. *Adv Sci* 8:2002658
- [6] Wang J, Liu L, Jiao S, Ma K, Lv J, Yang J (2020) Hierarchical carbon fiber@MXene@MoS₂ core-sheath synergistic microstructure for tunable and efficient microwave absorption. *Adv Funct Mater* 30:2002595
- [7] Liu P, Gao S, Zhang G, Huang Y, You W, Che R (2021) Hollow engineering to Co@N-doped carbon nanocages via synergistic protecting-etching strategy for ultrahigh microwave absorption. *Adv Funct Mater* 31:2102812
- [8] Zhang Y, Kong J, Gu J (2022) New generation electromagnetic materials: harvesting instead of dissipation solo. *Sci Bull* 67:1413–1415
- [9] Qin M, Zhang L, Wu H (2022) Dielectric loss mechanism in electromagnetic wave absorbing materials. *Adv Sci* 9:2105553
- [10] Wen B, Cao M, Lu M, Cao W, Shi H, Liu J, Wang X, Jin H, Fang X, Wang W, Yuan J (2014) Reduced graphene oxides: light-weight and high-efficiency electromagnetic interference shielding at elevated temperatures. *Adv Mater* 26:3484
- [11] Yan L, Hong C, Sun B, Zhao G, Cheng Y, Dong S, Zhang D, Zhang X (2017) In Situ growth of core-sheath heterostructural SiC nanowire arrays on carbon fibers and enhanced electromagnetic wave absorption performance. *ACS Appl Mater Interfaces* 9:6320–6331
- [12] Liu P, Gao S, Wang Y, Zhou F, Huang Y, Huang W, Chang N (2020) Core-shell Ni@C encapsulated by N-doped carbon derived from nickel-organic polymer coordination composites with enhanced microwave absorption. *Carbon* 170:503–516
- [13] Wang R, He M, Zhou Y, Nie S, Wang Y, Liu W, He Q, Wu W, Bu X, Yang X (2020) Metal–organic frameworks self-templated cubic hollow Co/N/C@MnO₂ composites for electromagnetic wave absorption. *Carbon* 156:378–388
- [14] Li Q, Zhang Z, Qi L, Liao Q, Kang Z, Zhang Y (2019) Toward the application of high frequency electromagnetic wave absorption by carbon nanostructures. *Adv Sci* 6:1801057
- [15] Meng X, He L, Liu Y, Yu Y, Yang W (2022) Carbon-coated defect-rich MnFe₂O₄/MnO heterojunction for high-performance microwave absorption. *Carbon* 194:207–219

- [16] Wang Y-Q, Zhao H-B, Cheng J-B, Liu B-W, Fu Q, Wang Y-Z (2022) Hierarchical $Ti_3C_2T_x@ZnO$ hollow spheres with excellent microwave absorption inspired by the visual phenomenon of eyeless urchins. *Nano micro Lett* 14:76
- [17] Ding J, Wang L, Zhao Y, Xing L, Yu X, Chen G, Zhang J, Che R (2019) Boosted interfacial polarization from multi-shell $TiO_2@Fe_3O_4@PPy$ heterojunction for enhanced microwave absorption. *Small* 15:1902885
- [18] Wu Y, Zhao Y, Zhou M, Tan S, Peymanfar R, Aslibeiki B, Ji G (2022) Ultrabroad microwave absorption ability and infrared stealth property of nano-micro $CuS@rGO$ lightweight aerogels. *Nano Micro Lett* 14:171
- [19] Wu Z, Cheng H-W, Jin C, Yang B, Xu C, Pei K, Zhang H, Yang Z, Che R (2022) Dimensional design and core-shell engineering of nanomaterials for electromagnetic wave absorption. *Adv Mater* 34:2107538
- [20] Liu M, Tian R, Chen H, Li S, Huang F, Peng K, Zhang H (2020) One-dimensional chain-like $MnO@Co/C$ composites for high-efficient electromagnetic wave absorbent. *J Magn Mater* 499:166289
- [21] Duan Y, Xiao Z, Yan X, Gao Z, Tang Y, Hou L, Li Q, Ning G, Li Y (2018) Enhanced electromagnetic microwave absorption property of peapod-like $MnO@carbon$ nanowires. *ACS Appl Mater Interfaces* 10:40078–40087
- [22] Yixuan H, Mukun H, Jinwen H, Panbo L, Zhongwu L, Zhonglei M, Wenbo J, Junwei G (2022) Hierarchical design of FeCo-based microchains for enhanced microwave absorption in C band. *Nano Res.* <https://doi.org/10.1007/s12274-022-5111-y>
- [23] Ding J, Song K, Gong C, Wang C, Guo Y, Shi C, He F (2022) Design of conical hollow ZnS arrays vertically grown on carbon fibers for lightweight and broadband flexible absorbers. *J Colloid Interface Sci* 607:1287–1299
- [24] Gong C, Jiang J, Ding J, Wang C, Guo Y, Shi C, He F (2022) Graphene oxide supported Yolk–Shell ZnS/Ni_3S_4 with the adjustable air layer for high performance of electromagnetic wave absorber. *J Colloid Interface Sci* 617:620–632
- [25] Xu D, Wu N, Le K, Wang F, Wang Z, Wu L, Liu W, Ouyang A, Liu J (2020) Bimetal oxide-derived flower-like heterogeneous $Co/MnO@C$ composites with synergistic magnetodielectric attenuation for electromagnetic wave absorption. *J Mater Chem C* 8:2451–2459
- [26] Zhao B, Guo X, Zhao W, Deng J, Fan B, Shao G, Bai Z, Zhang R (2017) Facile synthesis of yolk–shell $Ni@void@SnO_2(Ni_3Sn_2)$ ternary composites via galvanic replacement/Kirkendall effect and their enhanced microwave absorption properties. *Nano Res* 10:331–343
- [27] Xu H, Zhang G, Wang Y, Ning M, Ouyang B, Zhao Y, Huang Y, Liu P (2022) Size-dependent oxidation-induced phase engineering for MOFs derivatives via spatial confinement strategy toward enhanced microwave absorption. *Nano Micro Lett* 14:102
- [28] Li Z, Ottmann A, Zhang T, Sun Q, Meyer H-P, Vaynzof Y, Xiang J, Klingeler R (2017) Preparation of hierarchical $C@MoS_2@C$ sandwiched hollow spheres for lithium ion batteries. *J Mater Chem A* 5:3987–3994
- [29] Cheng F, Li W-C, Lu A-H (2016) Using confined carbonate crystals for the fabrication of nanosized metal oxide@carbon with superior lithium storage capacity. *J Mater Chem A* 4:15030–15035
- [30] Li Y, Li Y, Zhang Z, He X, Chen J, Liu C (2022) Pyrolysis kinetics of manganese carbonate. *J Therm Anal Calorim* 147:10801–10813
- [31] Yu H, Zeng Y, Li NW, Luan D, Yu L, Lou XW (2022) Confining Sn nanoparticles in interconnected N-doped hollow carbon spheres as hierarchical zincophilic fibers for dendrite-free Zn metal anodes. *Sci Adv* 8:eabm5766. <https://doi.org/10.1126/sciadv.abm5766>
- [32] Cui L, Tian C, Tang L, Han X, Wang Y, Liu D, Xu P, Li C, Du Y (2019) Space-confined synthesis of core-shell $BaTiO_3@carbon$ microspheres as a high-performance binary dielectric system for microwave absorption. *ACS Appl Mater Interfaces* 11:31182–31190
- [33] Yang M, Yuan Y, Li Y, Sun X, Wang S, Liang L, Ning Y, Li J, Yin W, Che R, Li Y (2020) Dramatically enhanced electromagnetic wave absorption of hierarchical CNT/Co/C fiber derived from cotton and metal-organic-framework. *Carbon* 161:517–527
- [34] Wang K, Chen Y, Tian R, Li H, Zhou Y, Duan H, Liu H (2018) Porous Co–C core-shell nanocomposites derived from Co-MOF-74 with enhanced electromagnetic wave absorption performance. *ACS Appl Mater Interfaces* 10:11333–11342
- [35] Wang Y, Ding X, Wang F, Li J, Song S, Zhang H (2016) Nanoconfined nitrogen-doped carbon-coated MnO nanoparticles in graphene enabling high performance for lithium-ion batteries and oxygen reduction reaction. *Chem Sci* 7:4284–4290
- [36] Yang L, Li H, Yu Y, Wu Y, Zhang L (2020) Assembled 3D MOF on 2D nanosheets for self-boosting catalytic synthesis of N-doped carbon nanotube encapsulated metallic Co electrocatalysts for overall water splitting. *Appl Catal B* 271:118939
- [37] Liu P, Zhang Y, Yan J, Huang Y, Xia L, Guang Z (2019) Synthesis of lightweight N-doped graphene foams with open reticular structure for high-efficiency electromagnetic wave absorption. *Chem Eng J* 368:285–298
- [38] Xiao Y, Wang X, Wang W, Zhao D, Cao M (2014) Engineering hybrid between MnO and N-doped carbon to

- achieve exceptionally high capacity for lithium-ion battery anode. *ACS Appl Mater Interfaces* 6:2051–2058
- [39] Sun Y, Hu X, Luo W, Xia F, Huang Y (2013) Reconstruction of conformal nanoscale MnO on graphene as a high-capacity and long-life anode material for lithium ion batteries. *Adv Funct Mater* 23:2436–2444
- [40] Zhou L, Cao H, Zhu S, Hou L, Yuan C (2015) Hierarchical micro-/mesoporous N- and O-enriched carbon derived from disposable cashmere: a competitive cost-effective material for high-performance electrochemical capacitors. *Green Chem* 17:2373–2382
- [41] Ren Y, Yan N, Feng J, Ma J, Wen Q, Li N, Dong Q (2012) Adsorption mechanism of copper and lead ions onto graphene nanosheet/ δ -MnO₂. *Mater Chem Phys* 136:538–544
- [42] Kang J, Min J, Kim S-I, Kim S-W, Jang J-H (2020) Three-level micro-meso-macroporous three-dimensional graphene for highly fast capacitive deionization. *Mater Today Energy* 18:100502
- [43] Fang Y, Wang W, Wang S, Hou X, Xue W, Zhao R (2022) A quantitative permittivity model for designing electromagnetic wave absorption materials with conduction loss: a case study with microwave-reduced graphene oxide. *Chem Eng J* 439:135672
- [44] Liang L, Li Q, Yan X, Feng Y, Wang Y, Zhang H-B, Zhou X, Liu C, Shen C, Xie X (2021) Multifunctional magnetic Ti₃C₂T_x MXene/graphene aerogel with superior electromagnetic wave absorption performance. *ACS Nano* 15:6622–6632
- [45] Kong L, Luo S, Zhang G, Xu H, Wang T, Huang J, Fan X (2022) Interfacial polarization dominant CNTs/PyC hollow microspheres as a lightweight electromagnetic wave absorbing material. *Carbon* 193:216–229
- [46] Wang H, Xiang L, Wei W, An J, He J, Gong C, Hou Y (2017) Efficient and lightweight electromagnetic wave absorber derived from metal organic framework-encapsulated cobalt nanoparticles. *ACS Appl Mater Interfaces* 9:42102–42110
- [47] Tao J, Tan R, Xu L, Zhou J, Yao Z, Lei Y, Chen P, Li Z, Ou JZ (2022) Ion-exchange strategy for metal-organic frameworks-derived composites with tunable hollow porous and microwave absorption. *Small Methods* 6:2200429
- [48] Yan X, Huang X, Zhong B, Wu T, Wang H, Zhang T, Bai N, Zhou G, Pan H, Wen G, Xia L (2020) Balancing interface polarization strategy for enhancing electromagnetic wave absorption of carbon materials. *Chem Eng J* 391:123538
- [49] Wei H, Tian Y, Chen Q, Estevez D, Xu P, Peng H-X, Qin F (2021) Microwave absorption performance of 2D iron-quinoid MOF. *Chem Eng J* 405:126637
- [50] Sun X, Li Y, Huang Y, Cheng Y, Wang S, Yin W (2022) Achieving super broadband electromagnetic absorption by optimizing impedance match of rGO sponge metamaterials. *Adv Funct Mater* 32:2107508
- [51] Lv H, Wu C, Tang J, Du H, Qin F, Peng H, Yan M (2021) Two-dimensional SnO/SnO₂ heterojunctions for electromagnetic wave absorption. *Chem Eng J* 411:128445
- [52] Pi K, McCreary KM, Bao W, Han W, Chiang YF, Li Y, Tsai SW, Lau CN, Kawakami RK (2009) Electronic doping and scattering by transition metals on graphene. *Phys Rev B* 80:075406
- [53] Sun M, Wang D, Xiong Z, Zhang Z, Qin L, Chen C, Wu F, Liu P (2022) Multi-dimensional Ni@C-CoNi composites with strong magnetic interaction toward superior microwave absorption. *J Mater Sci Technol* 130:176–183
- [54] Song Y, Yin F, Zhang C, Yu H, Jing W, Yuan Y (2020) Inverse-opal-based carbon composite monoliths for microwave absorption applications. *Carbon* 166:328–338
- [55] Liang J, Ye F, Cao Y, Mo R, Cheng L, Song Q (2022) Defect-engineered graphene/Si₃N₄ multilayer alternating core-shell nanowire membrane: a plainified hybrid for broadband electromagnetic wave absorption. *Adv Funct Mater* 32:2200141
- [56] Dong S, Lyu Y, Li X, Chen J, Zhang X, Han J, Hu P (2020) Construction of MnO nanoparticles anchored on SiC whiskers for superior electromagnetic wave absorption. *J Colloid Interface Sci* 559:186–196
- [57] Duan Y, Jiang B, Ma C, Wang X, Wang Y, Li R, Yang W, Li Y (2021) Construction of MnO-skeleton cross-linked by carbon nanotubes networks for efficient microwave absorption. *J Colloid Interface Sci* 602:778–788
- [58] Wang Y, Guan H, Du S, Wang Y (2015) A facile hydrothermal synthesis of MnO₂ nanorod-reduced graphene oxide nanocomposites possessing excellent microwave absorption properties. *RSC Adv* 5:88979–88988
- [59] Wang Y, Han B, Chen N, Deng D, Guan H, Wang Y (2016) Enhanced microwave absorption properties of MnO₂ hollow microspheres consisted of MnO₂ nanoribbons synthesized by a facile hydrothermal method. *J Alloy Compd* 676:224–230
- [60] Liao Y, He G, Duan Y (2021) Morphology-controlled self-assembly synthesis and excellent microwave absorption performance of MnO₂ microspheres of fibrous flocculation. *Chem Eng J* 425:130512
- [61] Hu P, Dong S, Li X, Chen J, Zhang X, Hu P, Zhang S (2019) A low-cost strategy to synthesize MnO nanorods anchored on 3D biomass-derived carbon with superior microwave absorption properties. *J Mater Chem C* 7:9219–9228
- [62] Wang Y, Zhong W, Zhang S, Zhang X, Zhu C, Zhang X, Zhang X, Chen Y (2022) Pearl necklace-like CoMn-based nanostructures derived from metal-organic frames for

enhanced electromagnetic wave absorption. Carbon 188:254–264

- [63] Chen T, Jiang S, Li L, Qian K, Sun J, Guo W, Cai X, Yu K (2022) Vertically aligned MnO₂ nanostructures on carbon fibers with tunable electromagnetic wave absorption performance. Appl Surf Sci 589:152858
- [64] Jia H, Xing H, Ji X, Gao S (2021) Self-template and in-situ polymerization strategy to lightweight hollow MnO₂@-polyaniline core-shell heterojunction with excellent microwave absorption properties. Appl Surf Sci 537:147857

Publisher's Note Springer Nature remains neutral with regard to jurisdictional claims in published maps and institutional affiliations.

Springer Nature or its licensor (e.g. a society or other partner) holds exclusive rights to this article under a publishing agreement with the author(s) or other rightsholder(s); author self-archiving of the accepted manuscript version of this article is solely governed by the terms of such publishing agreement and applicable law.